# INSTITUTE FOR FUSION STUDIES

DOE/ET-53088-471 IFSR #471

## Studies of Plasma Equilibrium and Transport in a Tokamak Fusion Device with the Inverse-Variable Technique

R.R. KHAYRUTDINOV[a] AND V.E. LUKASH
Institute for Fusion Studies
The University of Texas at Austin
Austin, Texas 78712

January 1991

[a] *permanent address: I.V. Kurchatov Institute of Atomic Energy, Moscow, U.S.S.R.*

# THE UNIVERSITY OF TEXAS


# AUSTIN

# Studies of Plasma Equilibrium and Transport in a Tokamak Fusion Device with the Inverse-Variable Technique

R. R. Khayrutdinov[a)]
Institute for Fusion Studies
The University of Texas at Austin
Austin, Texas 78712
and
V. E. Lukash
I.V. Kurchatov Institute of Atomic Energy
Moscow, U.S.S.R

**Abstract**

We describe an accurate and efficient model for studying the evolution of tokamak plasmas. The equilibrium problem for a plasma with a free boundary is solved using the "inverse variable" technique. The one-dimensional (averaged on magnetic surfaces) system of transport equations are solved together with the circuit equations for the vacuum vessel and the passive and active coils. As an example of the application of this method, we simulate the discharge in the T-3M Tokamak as it transiently evolves to a separatrix configuration.

[a)]Permanent address: I.V. Kurchatov Institute of Atomic Energy, Moscow, U.S.S.R.

# I. Introduction

A vertically elongated plasma cross-section is considered to be advantageous for achieving high-beta and high-current plasmas in tokamak devices. Tokamaks with divertor configurations and shaped, noncircular plasma cross-sections play an increasingly more important role in fusion research than conventional circular cross-section tokamaks. Present-day tokamaks like JET, JT-60, and DIII-D operate in divertor regimes. The next generation of tokamaks, like ITER, are being designed as devices with high elongation.

These tokamaks are more complicated than those with circular cross-section. There are a number of problems associated with these devices. The currents in the poloidal field coils must be carefully programmed to obtain the desired plasma current and configuration. Positional control problems have to be solved. An elongated plasma is generally unstable to an axisymmetric vertical displacement. Vacuum vessel and passive conductors are used to stabilize fast plasma motion; an active control system is necessary to keep plasma at the equilibrium position during the discharge. To gain a good understanding of these phenomena in tokamaks and to design devices with optimal characteristics, it is necessary to have appropriate tools for the numerical simulation of tokamak operation and behavior. Several codes exist to simulate axisymmetric tokamak plasmas in two-dimensional geometry [1-5]. One of the most complicated and extensive of these codes is the TSC code [6]. This code uses a considerable amount of computer time.

The present paper describes an accurate and efficient model to study toroidal plasma evolution in two-dimensional geometry. In this code (named DINA), the equilibrium problem of a plasma with a free boundary in an externally applied magnetic field is solved together with the one-dimensional (averaged on magnetic surfaces) system of transport equations. For the vacuum vessel and the passive and active coils, the circuit equations are solved. The code includes such effects as fuelling by pellet injection and heating by neutral beams and $\alpha$-

particles. The cold, neutral particles are modelled in the plane approximation. The effects of bootstrap and beam-driven currents are taken into account. The main difference between this model and others is the method that is employed for the solution of the equilibrium problem. The "inverse variable" technique [7] is used in the code DINA to find the coordinates of the equilibrium magnetic surfaces. This method permits the flux coordinates to be determined very quickly and accurately.

# II. Equilibrium and Transport Equations

The plasma equilibrium in a magnetic field is described by the following simple system of vector equations:

$$\nabla p = \frac{1}{c}[\mathbf{j} \times \mathbf{B}] \ , \tag{1}$$

$$\mathrm{curl}\, \mathbf{B} = \frac{4\pi}{c}\mathbf{j} \ , \tag{2}$$

$$\mathrm{div}\, \mathbf{B} = 0 \ , \tag{3}$$

where $p$ is the plasma pressure, $\mathbf{B}$ is the magnetic field, $\mathbf{j}$ is the current density, and $c$ is the speed of light. In an axisymmetric configuration, the magnetic field $\mathbf{B}$ can be expressed in terms of the poloidal flux function $\Psi$ and the poloidal current $F$ as

$$B = \frac{1}{2\pi r}[\nabla\Psi \times \mathbf{e}_\varphi] + \frac{2}{cr}F\mathbf{e}_\varphi \ , \tag{4}$$

where $\mathbf{e}_\varphi$ is the unit vector in the toroidal direction, and $(r, z, \varphi)$ are cylindrical coordinates centered on the axis of toroidal symmetry. The first term in Eq. (4) is the poloidal field $\mathbf{B}_p$, which lies in the cross-sectional plane $(r, z)$, whereas the second term is the toroidal field $\mathbf{B}_t$. Substituting $\mathbf{B}$ from Eq. (4) into Eq. (1), we have

$$\nabla p = \frac{1}{2\pi rc}\left(\nabla\Psi j_t - \frac{2}{cr}F\nabla F\right) \ , \tag{5}$$

where $j_t$ is the toroidal component of the current density. Using $\Psi$ as a variable to describe the flux surfaces, we can write $p$ and $F$ as functions of $\Psi$: viz., $p = p(\Psi)$, $F = F(\Psi)$, $\nabla p = p'\nabla\Psi$, $\nabla F = F'\nabla\Psi$, where the prime denotes a derivative with respect to $\Psi$. From Eq. (5), the toroidal component of the current density, $j_t$, can be written as

$$j_t = r2\pi cp' + \frac{1}{rc}(F^2)' \ . \tag{6}$$

Using simple mathematical relations we obtain from Eqs. (1)–(6):

$$\Delta^*\Psi \equiv r\frac{\partial}{\partial r}\left(\frac{1}{r}\frac{\partial\Psi}{\partial r}\right) + \frac{\partial^2\Psi}{\partial z^2} = -\frac{4\pi^2}{c}rj_t$$

or

$$\Delta^*\Psi = \frac{8\pi^2}{c}r\left(r2\pi cp' + \frac{1}{rc}(F^2)'\right) \ , \tag{7}$$

which is called the Grad-Shafranov equilibrium equation. Using the notation $\psi = \Psi/2\pi$ and $f = 2F/c$, Eq. (7) can be written in a more compact and convenient form:

$$\frac{1}{r}\Delta^*\psi = -\left(4\pi r\frac{dp}{d\psi} + \frac{1}{2r}\frac{df^2}{d\psi}\right) \ . \tag{8}$$

To solve this equation, it is necessary to specify the functions $p = p(\psi)$ and $f = f(\psi)$, which can be found from the transport equations and the magnetic field diffusion equation. We introduce the flux coordinate system $(\rho, \theta, \varphi)$ shown in Fig. 1, where $\rho = \sqrt{\Phi}$, with $\Phi$ the toroidal flux, $\Phi(\psi) = \int\int_{S_\psi} B_t\, dr dz$, and where $\theta$ and $\varphi$ are the poloidal and toroidal angles, and where $S_\psi$ is the area enclosed by the magnetic contour $\psi = \text{const.}$ in the $(r, z)$ plane.

# III. Averaging Technique

Since in tokamaks, the energy and particle transport along the magnetic surfaces is much greater than the transport across the magnetic surfaces, we can assume that densities and temperatures are constant on each magnetic surface.

Let $\rho$ be the label for the magnetic surface $S$; we define the average over $S$ of an arbitrary quantity $A$ by

$$\langle A \rangle = \frac{\partial}{\partial V} \int_S A \, dV = \frac{1}{V'} \int_S A \frac{dS}{|\nabla \rho|} ,$$

where

$$V' = \frac{\partial V}{\partial \rho} = \int_S \frac{dS}{|\nabla \rho|} ,$$

and $V$ is the volume enclosed inside the magnetic surface $S$. This average has the following properties:

$$\langle \operatorname{div} \mathbf{H} \rangle = \frac{\partial}{\partial V} \langle \mathbf{H} \cdot \nabla V \rangle \quad , \quad \forall \mathbf{H} , \tag{9}$$

$$\frac{d}{dt} \left( V' \langle A \rangle \right) = V' \left\langle \dot{A} \right\rangle + \frac{d}{d\rho} \langle A \mathbf{u}_\rho \cdot \nabla V \rangle \quad , \quad \forall A , \tag{10}$$

where $\dot{A}$ is the time derivative at a fixed point $(r, z)$, with $d/dt$ being the time derivative at fixed $\rho$. The vector $\mathbf{u}_\rho$ is the velocity of the constant $\rho$ surface, defined by

$$\dot{\rho} + \mathbf{u}_\rho \cdot \nabla \rho = 0 . \tag{11}$$

From Eq. (9), it can be deduced that

$$\frac{\partial V'}{\partial t} = \frac{d}{d\rho} \langle \mathbf{u}_\rho \cdot \nabla V \rangle . \tag{12}$$

Applying this averaging technique to the Braginskii transport equations [8], we obtain a system of one-dimensional transport equations with the respect to the "radial" coordinate $\rho$.

# IV. Averaged Transport Equations

## A. Magnetic field diffusion equation

The projection of Ohm's law on the magnetic field is

$$\mathbf{E} \cdot \mathbf{B} = \frac{\mathbf{j} \cdot \mathbf{B}}{\sigma''} . \tag{13}$$

Applying the averaging technique to Eq. (13) we obtain:

$$\frac{d\Phi}{d\rho}\dot{\Psi} - \frac{d\Psi}{d\rho}\dot{\Phi} = \frac{4\pi}{\sigma''}\left[J\frac{dF}{d\rho} - F\frac{dJ}{d\rho}\right] , \tag{14}$$

where $J(\rho) = \int\int_{S_\rho} j_t\, dr dz$ is the toroidal current inside the $S_\rho$ surface and $\sigma$ is the Spitzer conductivity:

$$J(\rho) = -\mu_0 \left\langle \frac{g_{22}}{\sqrt{g}} \right\rangle_\theta \frac{d\Psi}{d\rho} \quad , \quad F(\rho) = \mu_0 \left\langle \frac{g_{33}}{\sqrt{g}} \right\rangle_\theta \frac{d\Phi}{d\rho} ,$$

$$\mu_0 = \frac{c}{4\pi} \quad , \quad g_{22} = \left(\frac{\partial r}{\partial \theta}\right)^2 + \left(\frac{\partial z}{\partial \theta}\right)^2 \quad , \quad g_{33} = r^2 ,$$

and $\sqrt{g} = -\partial(r,z,\varphi)/\partial(\rho,\theta,\varphi)$ is the Jacobian for the transformation from cylindrical coordinates to flux coordinates. The angle-average of the quantity $A$ is

$$\langle A \rangle_\theta = \int_0^{2\pi} \frac{A(\theta)\, d\theta}{2\pi} .$$

Denoting $C_2 = \left\langle g_{22}/\sqrt{g} \right\rangle_\theta$, $\quad C_3 = 1/\left\langle \sqrt{g}/g_{33} \right\rangle_\theta$, and using $d\Phi/dt = 0$, we can write Eq. (14) as

$$\dot{\Psi} + \frac{4\pi}{\sigma''}\mu_0^2 C_3^2 \rho \frac{d}{d\rho}\left(-\frac{C_2}{C_3\rho}\frac{d\Psi}{d\rho}\right) = 0 . \tag{15}$$

## B. Density equation

The variation of the density of the $j^{th}$ ion species with time is described by the equation

$$\dot{n}_j + \mathrm{div}\,(n_j \mathbf{u}_j) = S_j , \tag{16}$$

where $S_j$ is the source term, $n_j$ is the density, and $\mathbf{u}_j$ is the flow velocity of the ion species. By averaging Eq. (16) over a magnetic surface, multiplying by $V'$, and using Eqs. (9) and (10), we obtain

$$\frac{d}{dt}(n_j V') + \frac{d}{d\rho}\langle n_j (\mathbf{u}_j - \mathbf{u}_\rho)\cdot\nabla\rho\rangle = \langle S_j \rangle V' . \tag{17}$$

Denoting the particle flux relative to a constant $\rho$ surface by $\Gamma_j = \langle n_j(\mathbf{u}_j - \mathbf{u}_\rho)\cdot\nabla\rho\rangle$, we compute Eq. (17) as:

$$\frac{d}{dt}(n_j V') + \frac{d}{d\rho}(\Gamma_j V') = \langle S_j \rangle V' . \tag{18}$$

## C. Energy equations

If the viscosity terms are neglected, the energy balance equation for the electrons can be written as

$$\frac{3}{2}\dot{p}_e + \text{div}\left(\mathbf{q}_e + \frac{5}{2}p_e\mathbf{u}_e\right) = \mathbf{jE} - Q_{ei} - \mathbf{u}_i\nabla p_i + Q_e \ , \tag{19}$$

where $p_e$ and $p_i$ are the electron and ion pressure, respectively; $\mathbf{q}_e$ is the electron heat flux; $Q_{ei}$ is the electron-ion heat exchange; $\mathbf{u}_e$ and $\mathbf{u}_i$ are the electron and ion flow velocity, respectively; and $Q_e$ is the source term. Due to plasma ambipolarity, we have $\mathbf{u}_e = \mathbf{u}_i$. From Ohm's law, namely,

$$\sigma''\left(\mathbf{E} + \frac{\mathbf{u}_e}{c}\times\mathbf{B}\right) = \mathbf{j} \ ,$$

it can be deduced that

$$\mathbf{j}\cdot\mathbf{E} = \frac{\mathbf{u}_e}{c}\cdot(\mathbf{j}\times B) + \frac{j^2}{\sigma''} = \mathbf{u}_e\cdot\nabla p + Q_{dg} \ , \tag{20}$$

where $Q_{dg} = j^2/\sigma''$.

Using Eq. (20) and averaging Eq. (19), we obtain

$$\frac{3}{2}\frac{1}{(V')^{2/3}}\frac{d}{dt}\left[p_e(V')^{5/3}\right] + \frac{d}{d\rho}\left[\left(q_e + \frac{5}{2}T_e\Gamma_e\right)V'\right] - \frac{\Gamma_e}{n_e}V'\frac{d}{d\rho}(p_e) =$$

$$V'\left\langle -Q_{ei} + Q_{dg} + Q_e\right\rangle \ , \tag{21}$$

where $q_e = \langle\mathbf{q}_e\cdot\nabla\rho\rangle$.

The energy balance equation for the ions is

$$\frac{3}{2}\dot{p}_i + \text{div}\left(\mathbf{q}_i + \frac{5}{2}p_i\mathbf{u}_i\right) = Q_{ei} + \mathbf{u}_i\cdot\nabla p_i + Q_i \ . \tag{22}$$

Averaging Eq. (22) over a magnetic surface leads to

$$\frac{3}{2}\frac{1}{(V')^{2/3}}\frac{d}{dt}\left[p_i(V')^{5/3}\right] + \frac{d}{d\rho}\left[\left(q_i + \frac{5}{2}T_i\Gamma_i\right)V'\right] - \frac{\Gamma_e}{n_e}V'\frac{d}{d\rho}(p_i) = V'\left\langle Q_{ei} + Q_i\right\rangle \ , \tag{23}$$

where $q_i = \langle\mathbf{q}_i\cdot\nabla\rho\rangle$.

We will use simplified expressions for $\Gamma_j$, $q_e$, and $q_i$ that correspond to the so-called "diagonal" model. In the diagonal model, we assume that

$$\mathbf{q}_i = -\chi_i n_i \nabla T_i \qquad \text{and} \qquad \mathbf{q}_e = -\chi_e n_e \nabla T_e \ ,$$

where $\chi_i$ and $\chi_e$ are the electron and ion thermal conductivities, respectively. The particle flux of ion species $j$ can be written as

$$\mathbf{\Gamma}_j = n_j(\mathbf{u}_j - \mathbf{u}_\rho) = -D\nabla n_j + n_j \mathbf{V}_p \ , \tag{24}$$

where $D$ is the diffusion coefficient and $\mathbf{V}_p$ is the inward pinch velocity. The averaged fluxes are given by

$$\begin{aligned} q_i &= -\chi_i n_i \left\langle \nabla\rho^2 \right\rangle \frac{dT_i}{d\rho} \ , \\ q_e &= -\chi_e n_e \left\langle \nabla\rho^2 \right\rangle \frac{dT_e}{d\rho} \ , \end{aligned} \tag{25}$$

and

$$\Gamma_j = -D \left\langle \nabla\rho^2 \right\rangle \frac{dn_j}{d\rho} + n_j \left\langle \mathbf{V}_p \cdot \nabla\rho \right\rangle \ . \tag{26}$$

The coefficients $D$, $\chi_i$, $\chi_e$, and $V_p$ are functions of the plasma parameters and their gradients; here, $j$ denotes either deuterium, tritium, hydrogen; and $Q_{ei}$ is given by

$$Q_{ei} = 3\,\frac{m_e}{m_i}\frac{n_e}{\tau_e}(T_e - T_i) \ ,$$

where $\tau_e$ is the collision time for electrons [8]. The energy sources are $Q_e = Q_{e\alpha} - Q_{eR} + Q_{e\ \mathrm{aux}}$ and $Q_i = Q_{i\alpha} + Q_{i\ \mathrm{aux}}$, where $Q_{e\alpha}$ and $Q_{i\alpha}$ are the $\alpha$ particle heating power to electrons and ions, respectively; $Q_{eR}$ is the radiation power (bremsstrahlung and cyclotron); $Q_{e\ \mathrm{aux}}$ and $Q_{i\ \mathrm{aux}}$ are the auxiliary heating power to the electrons and ions, respectively. The source terms $S_j$ takes into consideration fuelling (for example, by pellet injection). The energy source term profile is calculated with the help of a neutral beam injection model in the thin beam approximation, with the two-dimensional magnetic surface geometry taken into account. The other heating methods are modelled parametrically in the energy source terms.

The toroidal flux in the plasma varies with time, and thus $\rho_{\max}$ is not constant. The $\rho$ variable is constrained to the interval $[0, \rho_{\max}]$. We define the normalized variable $\overline{\rho} = \rho/\rho_{\max}$. Then the time derivative can be written as

$$\frac{d}{dt} - \frac{\overline{\rho}}{\rho_{\max}} \frac{d\rho_{\max}}{dt} \frac{d}{d\overline{\rho}} ,$$

The Jacobian becomes $\sqrt{g} = \sqrt{g}(\overline{\rho})/\rho_{\max}$, and

$$V'(\rho) = V'(\overline{\rho})\rho_{\max} ,$$

$$C_2(\rho) = C_2(\overline{\rho})\rho_{\max} ,$$

$$C_3(\rho) = C_3(\overline{\rho})\rho_{\max} ,$$

$$\langle \nabla\rho \rangle^2 = \rho_{\max}^2 \left\langle \nabla\overline{\rho}^2 \right\rangle ,$$

$$\langle |\nabla\rho| \rangle = \rho_{\max} \langle |\nabla\overline{\rho}| \rangle ,$$

$$f(\rho) = C_3(\overline{\rho})\rho_{\max}^2 \overline{\rho}/\pi . \tag{27}$$

## D. Summary of transport equations

Using Eqs. (14), (17), (20), (22), (24), (25), and (26), we obtain the following system of transport equations:

Magnetic field diffusion:

$$\frac{d\Psi}{dt} - \frac{\overline{\rho}}{\rho_{\max}} \frac{d\rho_{\max}}{dt} \frac{d\Psi}{d\overline{\rho}} + \frac{4\pi}{\sigma''} \mu_0^2 C_3^2 \overline{\rho} \frac{d}{d\overline{\rho}} \left( -\frac{C_2}{C_3\overline{\rho}} \frac{d\Psi}{d\overline{\rho}} \right) = 0 . \tag{28}$$

Balance of $j$ particles:

$$\rho_{\max} \frac{d}{dt} \left( \frac{n_j V'}{\rho_{\max}} \right) - \frac{\overline{\rho}}{\rho_{\max}} \frac{d\rho_{\max}}{dt} \frac{d}{d\overline{\rho}} (n_j V') + \frac{d}{d\overline{\rho}} (V'\Gamma_j) = V' \langle S_j \rangle . \tag{29}$$

Energy balance for electrons:

$$\frac{3}{2}\frac{\rho_{\max}^{5/3}}{V'^{2/3}}\frac{d}{dt}\left(\frac{n_eT_eV'^{5/3}}{\rho_{\max}}\right)-\frac{3}{2V'^{2/3}}\frac{\overline{\rho}}{\rho_{\max}}\frac{d\rho_{\max}}{dt}\frac{d}{d\overline{\rho}}\left(n_eT_eV'^{5/3}\right)+\frac{5}{2}\frac{d}{d\overline{\rho}}\left(V'\Gamma_eT_e\right)-$$

$$\frac{\Gamma_eV'}{n_e}\frac{d}{d\overline{\rho}}\left(n_eT_e\right)-\frac{d}{d\overline{\rho}}\left(V'\chi_en_e\left\langle\nabla\overline{\rho}^2\right\rangle\frac{dT_e}{d\overline{\rho}}\right)=\left\langle Q_{dg}+Q_e-Q_{ei}\right\rangle V'\ . \tag{30}$$

Energy balance for ions :

$$\frac{3}{2}\frac{\rho_{\max}^{5/3}}{V'^{2/3}}\frac{d}{dt}\left(\frac{n_iT_iV'^{5/3}}{\rho_{\max}}\right)-\frac{3}{2V'^{2/3}}\frac{\overline{\rho}}{\rho_{\max}}\frac{d\rho_{\max}}{dt}\frac{d}{d\overline{\rho}}\left(n_iT_iV'^{5/3}\right)+\frac{5}{2}\frac{d}{d\overline{\rho}}\left(V'\Gamma_iT_i\right)-$$

$$\frac{\Gamma_eV'}{n_e}\frac{d}{d\overline{\rho}}\left(n_iT_i\right)-\frac{d}{d\overline{\rho}}\left(V'\chi_in_i\left\langle\nabla\overline{\rho}^2\right\rangle\frac{dT_i}{d\overline{\rho}}\right)=\left\langle Q_i+Q_{ei}\right\rangle V'\ , \tag{31}$$

where $\Gamma_j(\overline{\rho})=-D\left\langle\nabla\overline{\rho}^2\right\rangle dn_j/d\overline{\rho}+n_j\left\langle V_p|\nabla\overline{\rho}|\right\rangle$, $\Gamma_e=\sum_j\Gamma_j$, $n_e=\sum_j n_jz_j+n_\alpha z_\alpha$, $n_\alpha$ is the density of $\alpha$ particles, and $z_j$ is the charge of the $j^{th}$ particle species.

# V. Numerical Solution of the Model

Equations (28)–(31) form a system of second-order, quasilinear, parabolic equations. In solving these equations we use an implicit scheme with iteration in the nonlinearities. The equilibrium, Eq. (8), is solved by the inverse variable technique with the use of the POLAR code [7]. The profiles of $dp(\overline{\rho})/d\overline{\rho}$, $d\Psi(\overline{\rho})/d\overline{\rho}$, and $q(\overline{\rho})$, which are used in the equilibrium problem, are obtained from the solution of the transport equations.

From the solution of the equilibrium equation we obtain the coordinates $r(\overline{\rho},\theta)$ and $z(\overline{\rho},\theta)$ of the magnetic surfaces. By averaging over the magnetic surfaces, we obtain the metric coefficients $C_2(\overline{\rho})$, $C_3(\overline{\rho})$, $\langle\nabla\overline{\rho}^2\rangle$, $\langle|\nabla\overline{\rho}|\rangle$, and $V'$. The value $\rho_{\max}$ is calculated with Eq. (27). Then the transport equations are solved with these coefficients. We obtain the profiles $dp/d\overline{\rho}$, $d\Psi/d\overline{\rho}$, and $q(\overline{\rho})$ for the next time step. With these parameters, a new equilibrium is calculated. Since the metric coefficients depend on time, several iterations are carried out, so that more exact profiles of $dp/d\overline{\rho}$, $d\Psi/d\overline{\rho}$, and $q(\overline{\rho})$ and the magnetic surface

coordinates are obtained. A schematic flow-diagram of the various calculations is shown in the Appendix.

For the case of an external magnetic field with a free boundary plasma, the principle of "Virtual Casing" [9] is used to find the flux and the magnetic field produced by the plasma current.

## A. Boundary conditions

For the densities and energies, it is appropriate to use either mixed boundary conditions

$$\alpha\xi + \beta \frac{d\xi}{d\overline{\rho}} = \gamma\Big|_{\overline{\rho}=1} , \tag{32}$$

where $\alpha$, $\beta$, and $\gamma$ are coefficients and $\xi$ successively denotes $n_j$, $T_i$, and $T_e$; or Dirichlet boundary conditions, where the values $n_j^0$, $T_i^0$, and $T_e^0$ are specified on the plasma boundary.

The boundary condition for the magnetic field diffusion equation is

$$-\frac{1}{c}\frac{d\Psi_b}{dt} = -\frac{1}{c}\frac{d\Psi_{pl}}{dt} - \frac{1}{c}\frac{d\Psi^{\text{ext}}}{dt} , \tag{33}$$

where $\Psi_b$ is $\Psi$ on the plasma boundary; $\Psi_{pl}$ is the plasma current flux; and $\Psi^{\text{ext}}$ denotes the total poloidal flux produced by the poloidal field currents and by the eddy currents induced in the vacuum vessel and in the axisymmetric conductors.

We define the plasma self-inductance by the equation $L_p = \Psi_{pl}/I_{pl}$, where $I_{pl}$ is the total plasma current. We can write Eq. (33) as

$$\frac{d\Psi_b}{dt} = \frac{d\Psi^{\text{ext}}}{dt} + \frac{d}{dt}\left(L_p I_{pl}\right) . \tag{34}$$

Using an implicit scheme for the discretization of Eq. (34), we obtain

$$\frac{\Psi_b - \widehat{\Psi}_b}{\tau} = \frac{\Psi^{\text{ext}} - \widehat{\Psi}^{\text{ext}}}{\tau} + \frac{\left(L_p I_{pl} - \widehat{L}_p \widehat{I}_{pl}\right)}{\tau} , \tag{35}$$

where the caret denotes values from the previous time-step. Using the relation $I_{pl} = -\mu_0 C_2 d\Psi/d\overline{\rho}\Big|_{\overline{\rho}=1}$ we can write:

$$\mu_0 C_2 \frac{d\Psi}{d\overline{\rho}}\,|_b + \Psi_b = \widehat{\Psi}_b + \Psi^{\text{ext}} - \widehat{\Psi}^{\text{ext}} - \widehat{L}_p \widehat{I}_{pl} . \tag{36}$$

Equation (36) constitutes the mixed boundary condition for the $\Psi$ equation.

## B. Transport coefficients

Since the radial dependence of the electron thermal conductivity is not presently known, we use the following simple form for $\chi_e$:

$$\chi_e = \beta(1 + \delta\overline{\rho}^2) \ ,$$

where $\beta$ and $\delta$ are adjustable coefficients. The value of $\delta$ is chosen to define a wide or narrow temperature profile, and the value of $\beta$ is calculated at each time-step so that we obtain a global energy confinement time identical to the assumed scaling law (e.g., Kay-Goldston, Alcator, etc.).

The thermal conductivity $\chi_i$ of the ions is either assumed to be neoclassical [10] or considered to be equal to the electron thermal conductivity. We assume that the particle diffusion coefficient is proportional to the electron thermal conductivity $D \simeq 0.2\chi_e$ and that the inward pinch velocity is given by $V_p = k_p D\overline{\rho}/a$, where $a$ is the plasma minor radius and $k_p$ is chosen to obtain the required density profile.

A fusion reactor that operates in a continuous regime is supposed to use non-inductive methods for maintaining the plasma current to be constant. In a high temperature plasma, the value of the bootstrap current can be significant. Therefore we include in our model the neoclassical bootstrap current and beam-driven current effects. After inclusion of driven and bootstrap currents, the magnetic diffusion equation is modified as follows:

$$\frac{d\Phi}{d\overline{\rho}}\,\dot{\Psi} - \frac{d\Psi}{d\overline{\rho}}\,\dot{\Phi} = \frac{4\pi}{\sigma}\left(J\frac{dF}{d\overline{\rho}} - F\frac{dJ}{d\overline{\rho}}\right) + \langle \mathbf{j}\cdot\mathbf{B}\rangle\,\frac{V'c}{\sigma} \ , \tag{37}$$

where $\sigma = \sigma'' - \alpha\sigma''$; $\alpha$ is the neoclassical trapping term [10]; and $\langle \mathbf{j}\cdot\mathbf{B}\rangle = \langle \mathbf{j}\cdot\mathbf{B}\rangle_{\rm boot} + \langle \mathbf{j}\cdot\mathbf{B}\rangle_{\rm beam}$, where $\langle \mathbf{j}\cdot\mathbf{B}\rangle_{\rm boot}$ and $\langle \mathbf{j}\cdot\mathbf{B}\rangle_{\rm beam}$ are the bootstrap and beam-driven terms, respectively.

## C. The circuit equations

In a solid conductor, we can write Ohm's law in the simple form

$$j_t = \sigma E_t \ ,$$

where $E_t$ is the toroidal component of the electric field. In the $i^{th}$ element of a conductor, i.e., with coordinates $(r_i, z_i)$, we have $E_t^i = -\dot{\Psi}_i + V_i/2\pi r_i$, where $V_i$ is the voltage applied to the $i^{th}$ circuit. From Ohm's law we obtain

$$-\dot{\Psi}_i + V_i = \frac{2\pi r_i j_i}{\sigma_i} \ . \tag{38}$$

If we assume that the current density $j_i$ is homogeneous in the area $S_i$ of the conductor, then Eq. (38) can be re-expressed as

$$-\dot{\Psi}_i + V_i = R_i I_i \tag{39}$$

where $R_i = 2\pi r_i/\sigma_i S_i$ is the resistivity of the element $S_i$.

The poloidal flux $\Psi_i$ on each $i^{th}$ element is determined by the sum

$$\Psi_i = L_i I_i + \sum_{j \neq i} M_{ij} I_j + \Psi_{pl}^i \ , \tag{40}$$

where $M_{ij}$ is the mutual inductance between the $i^{th}$ and $j^{th}$ elements (proportional to the Green's function for the elliptic operator $\Delta^*$); $L_i$ is the self-inductance of the $i^{th}$ element; and $\Psi_{pl}^i$ is the flux created by the plasma current in the $i^{th}$ element. Using Eq. (39) and Eq. (38), we obtain the circuit equation

$$\frac{d}{dt}\left( L_i I_i + \sum_{j \neq i} M_{ij} I_j + \Psi_{pl}^i \right) + R_i I_i = V_i \ . \tag{41}$$

Note that in the case of a vacuum vessel and passive coils, the value $V_i$ is equal to zero.

In conventional tokamaks, four types of poloidal field coils exist:

- Current ramp-up and Ohmic heating coils,
- Vertical field coils,
- Shaping coils, and
- Plasma position control coils.

# VI. Application to the T-3M Tokamak

As an illustration of the application of this numerical scheme, we present here a simulation of the operation in the T-3M tokamak. In this machine the plasma evolves from the limiter regime to the divertor regime. The plasma configuration has two $X$-points inside the vacuum vessel.

The T-3M poloidal field coil system is shown in Fig. 2. Coils 1, 2, and 4 are inductor coils, and coils 3 and 5 are vertical field coils. In the flat-top regime the plasma current is $I_{pl} = 200\,\mathrm{kA}$ and the current in the inductor is $I_{\mathrm{ind}} = -0.1 I_{pl} = -20\,\mathrm{kA}$.

We present the results of two operational scenarios. In the first scenario, the plasma current remains approximately constant. In the second scenario, the plasma current decreases from $I_{pl} = 200\,\mathrm{kA}$ to 95 kA. The time for the transition to the divertor configuration is 10 ms. The initial plasma shape and magnetic surface contours when the plasma is limited by the vessel are presented in Fig. 2. To create the divertor configuration, the current in coil 4 is changed from negative to positive. The plasma current $I_{pl}$ decreases during this process (second scenario). To compensate the poloidal flux change at the plasma boundary and to maintain the plasma current constant, we induce a negative current in coil 9. This leads to the first scenario. In the first scenario the temperature, current, and density profiles remain monotonic. In coil 4 the current changes from $-20$ to $+30\,\mathrm{kA}$, and in coil 9 we have to induce a current of $-30\,\mathrm{kA}$. The time evolution of the currents and the flux-surface contours in the final state are shown in Figs. 4 and 5, respectively. In the second scenario, the density and

temperature profiles remain monotonic, but the current becomes peaked during the plasma current delay. The current profiles at three different times are plotted in Fig. 6. The current evolution in the coils and the behaviour of the safety factor, $q_a$, at the plasma edge are illustrated in Figs. 7 and 8, respectively. It is seen that when the plasma detaches from the vessel, the value of $q_a$ increases; however, when plasma becomes limited by the separatrix, the value of $q_a$ decreases. The plasma shape at the final state is shown in Fig. 9. The initial and final plasma parameters are shown in Table 1.

The numerical simulation of a single scenario requires about 30 minutes on a VAX computer. The time step used here was 0.1 ms. The plasma mesh contained 24 radial and 66 angle points.

# VII. Summary

We have described a $1-\frac{1}{2}$ D code (DINA) for the simulation of the evolution of free-boundary toroidal plasmas in time-dependent external magnetic fields. Using this code we are able to simulate plasma motion, including the effects of eddy currents in the vacuum vessel, poloidal field coils, and axisymmetric conductors. We can study the behaviour of the plasma, which is unstable in the vertical and horizontal directions, and simulate the control of the plasma position using active feedback control system. This code is faster and simpler than other $1-\frac{1}{2}$ D codes, and it permits the simulation of all the main characteristics of tokamak plasmas.

## Acknowledgments

The authors thank V. Drozdov for providing the POLAR code and offering assistance in its running. We also appreciates useful discussions and help provided by the members of the IGNITEX group, especially R. Carrera, E. Montalvo, and J. Dong. This work was supported by the U.S. Department of Energy Contract #DE-FG05-80ET-53088.

## Table I. Plasma Parameters

| parameter | initial | first scenario | second scenario |
|---|---|---|---|
| plasma current, kA | 200 | 195. | 95. |
| plasma elongation | 1.4 | 2.1 | 1.8 |
| minor radius, cm | 20. | 12. | 10. |
| major radius, cm | 106. | 106. | 106. |
| safety factor on plasma axis | 1.1 | 1.2 | 1.3 |
| $q$ at the plasma edge | 4.5 | 2.9 | 3.5 |
| current density on axis, kA/cm$^2$ | 0.35 | 0.42 | 0.36 |
| electron temperature on axis, eV | 580. | 730. | 650. |
| ion temperature on axis, eV | 500. | 550. | 530. |
| average plasma density, $10^{13}$/cm$^3$ | 4.5 | 6.1 | 6.8 |
| toroidal field on axis, $T$ | 3. | 3. | 3. |
| internal inductance | 1.06 | 0.61 | 0.95 |

## Appendix Scheme of Calculations

initial values :
$p(\overline{\rho}), \Psi(\overline{\rho}), q(\overline{\rho}), n_j(\overline{\rho}), T_e(\overline{\rho}), T_i(\overline{\rho}), \cdots$

Equilibrium :
obtain coordinates
$r(\overline{\rho}, \theta), z(\overline{\rho}, \theta)$

obtain metric coefficients :
$\rho_{\max}, C_2, C_3, \langle \nabla \overline{\rho}^2 \rangle, \langle |\nabla \overline{\rho}| \rangle, V'(\overline{\rho})$

transport :
internal iterations
obtain profiles of
$p(\overline{\rho}), \Pi(\overline{\rho}), q(\overline{\rho}), n_j(\overline{\rho}), T_{e,i}(\overline{\rho}), dp/d\overline{\rho}, d\Psi/d\overline{\rho}$

No:
external
iterations

Is the required accuracy satisfied?

Yes:

New time step:

## References


[1] Helton, F.J., Miller, R.L., and Rawls, J.M., "Two-Dimensional Multi-Fluid Tokamak Transport Code," J. Comp. Phys. **24**, 117 (1977).

[2] Byrne, N.R., and Klein, H.H., "G2M a Two-Dimensional Diffusion Time Scale Tokamak Code," J. Comp. Phys. **26**, 352 (1978)

[3] Hogan, J.T., "The Accessibility of High Beta Tokamak States," Nucl. Fusion **19**, 753 (1979).

[4] Turnbull, A.D., and Storer, R.G., "A Plasma Resistive Diffusion Model," J. Comp. Phys. **50**, 409 (1983).

[5] Blum, J., and Le Foll, J., "Plasma Equilibrium Evolution at the Resistive Diffusion Timescale," Comp. Phys. Rep. **1**, 465 (1984).

[6] Jardin, S.C., Pomphrey, N., and DeLucia, J., "Dynamic Modeling of Transport and Positional Control of Tokamaks," J. Comp. Phys. **66**, 481 (1986).

[7] Degtyarev, L.M., and Drozdov, V.V., "An Inverse Variable Technique in the MHD-Equilibrium Problem," Comp. Phys. Reports **2**, 341 (1985).

[8] Braginskii, S.I., in *Reviews of Plasma Physics* (Consultants Bureau, New York, 1965), Vol. 1, p. 205-311.

[9] Zakharov, L.E., and Shafranov, V.D., in *Reviews of Plasma Physics* (Consultants Bureau, New York, 1986), Vol. 11, p. 178-180.

[10] Hinton, F.L., and Hazeltine, R.D., "Theory of Plasma Transport in Toroidal Confinement Systems," Rev. Mod. Phys. **48**, 239 (1976).

## Figure Captions

1. Flux coordinate system: poloidal angle $\theta$, toroidal angle $\varphi$, and surface coordinate $\rho$.

2. Poloidal field coil system of the T3-M Tokamak. Coils 1, 2 and 4 are inductor coils, coil 6 is the vertical field coil, coils 3 and 5 are control coils, and coils 7 and 8 are fast control coils.

3. Initial state of the plasma magnetic surfaces.

4. Time evolution of the coil currents in the first scenario.

5. Final state of the plasma magnetic surfaces (first scenario).

6. Plasma current profiles at various times (second scenario).

   (1) $t = 0$, $I_p = 200\,\mathrm{kA}$
   (2) $t = 5\,\mathrm{ms}$, $I_p = 135\,\mathrm{kA}$
   (3) $t = 10\,\mathrm{ms}$, $I_p = 95\,\mathrm{kA}$

7. Time evolution of the coil currents in the second scenario.

8. Evolution of the safety factor at the plasma edge.

9. Final state of the plasma magnetic surfaces (second scenario).

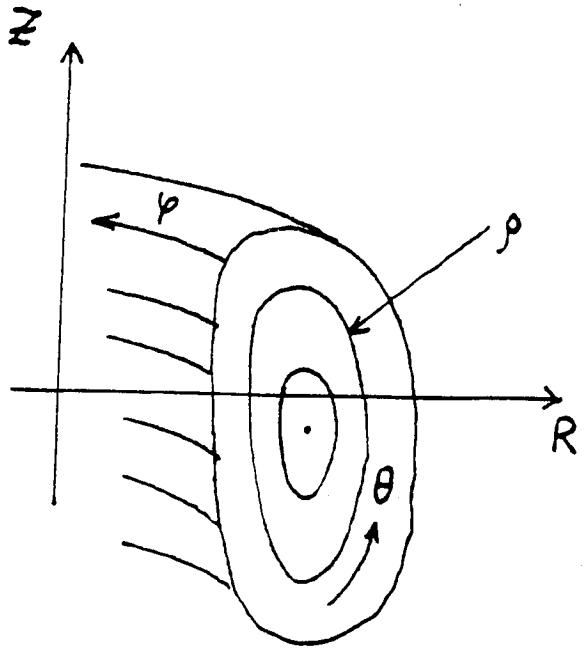


**Fig.**1

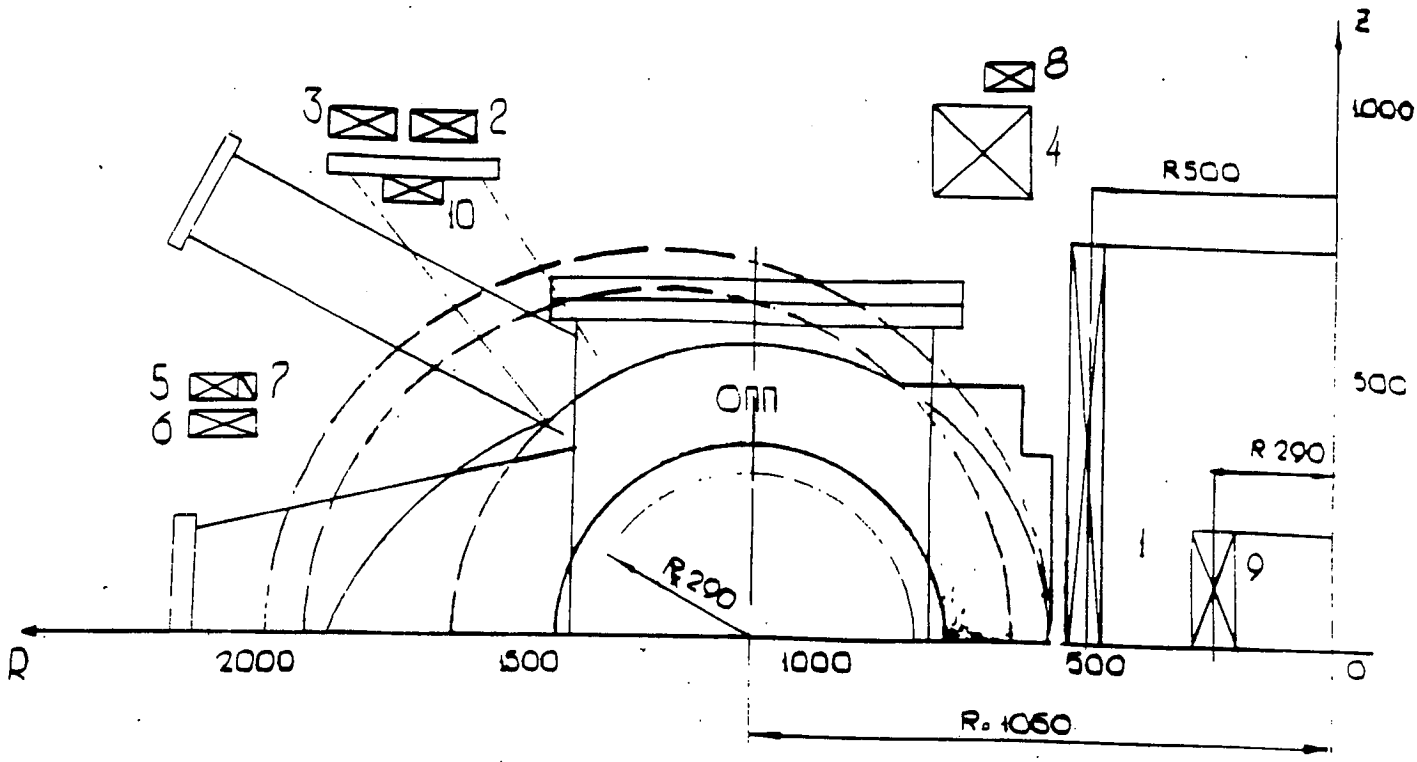
Z
1000
500
R500
R 290
R200
ОПП
R
2000
1500
1000
500
0
R₀ 1060
1
2
3
4
5
6
7
8
9
10

**Fig.2**

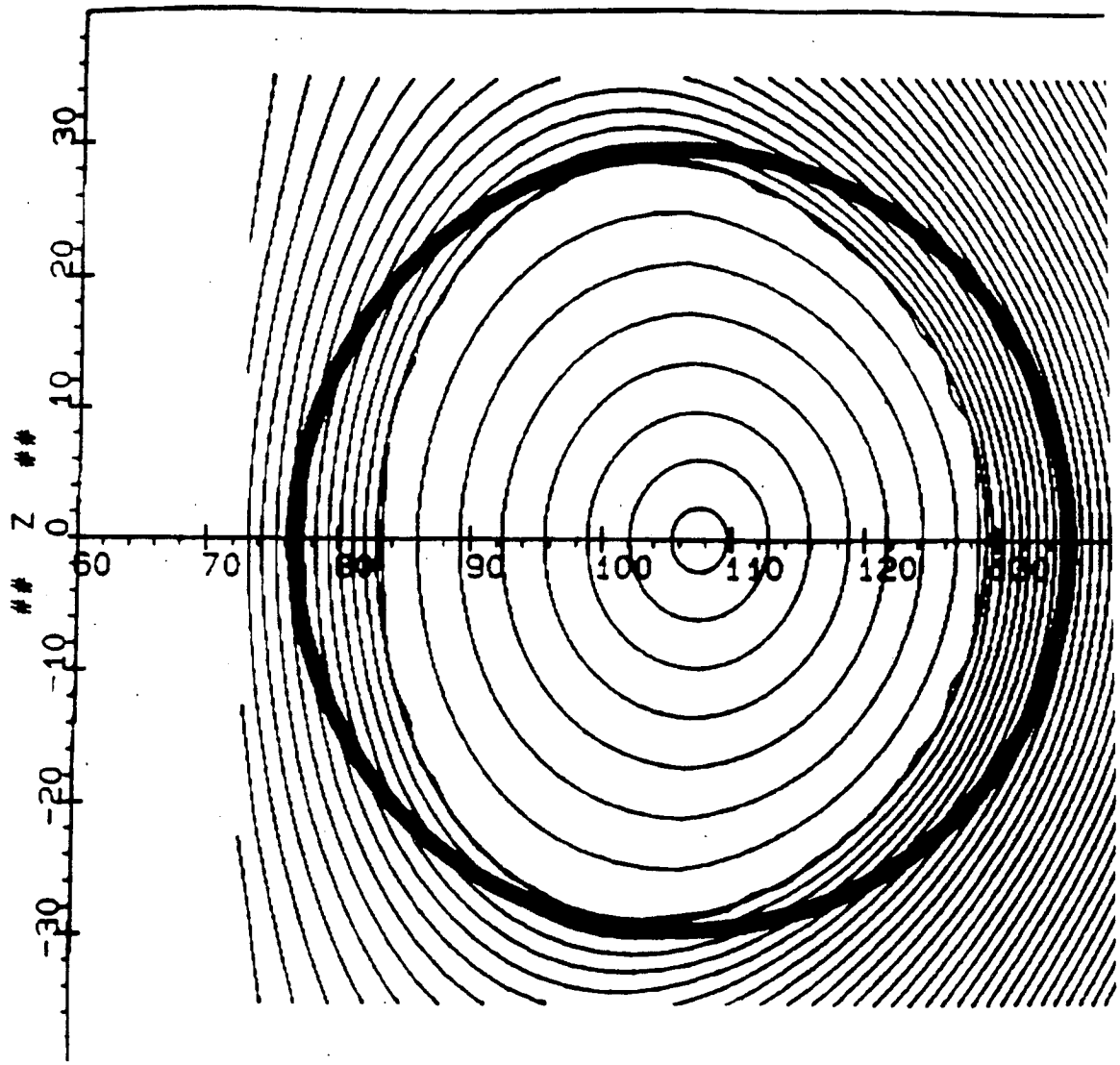


Fig.3

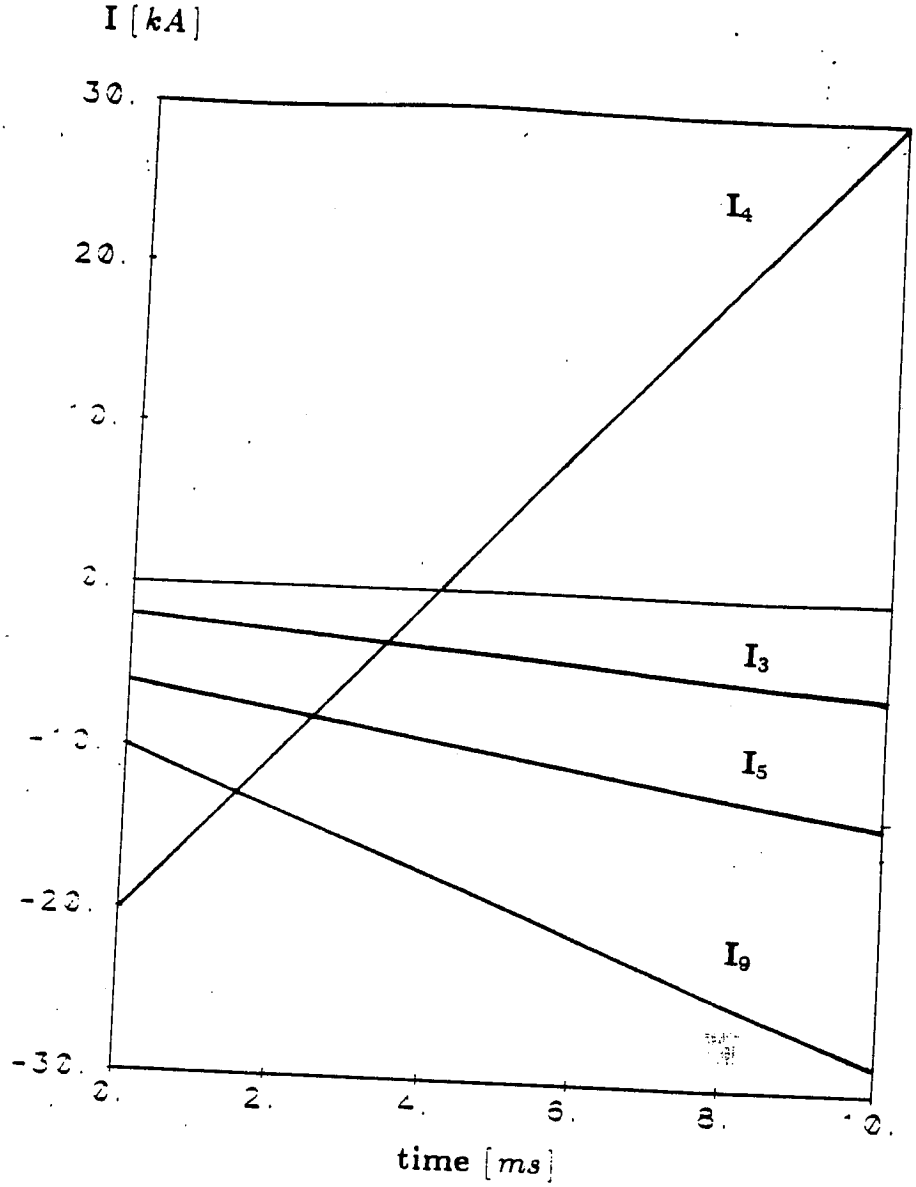


**Fig.**4

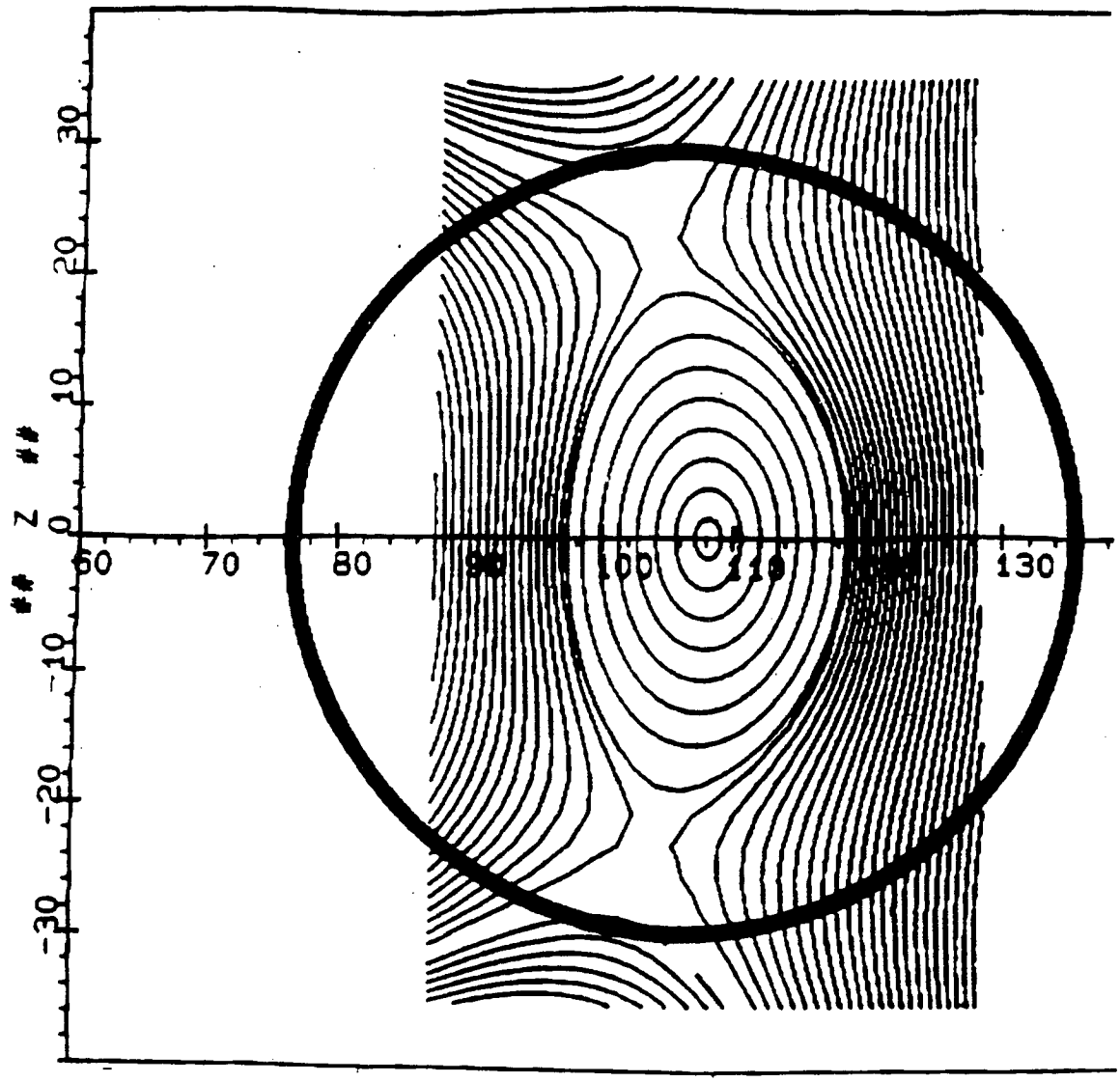


Fig.5

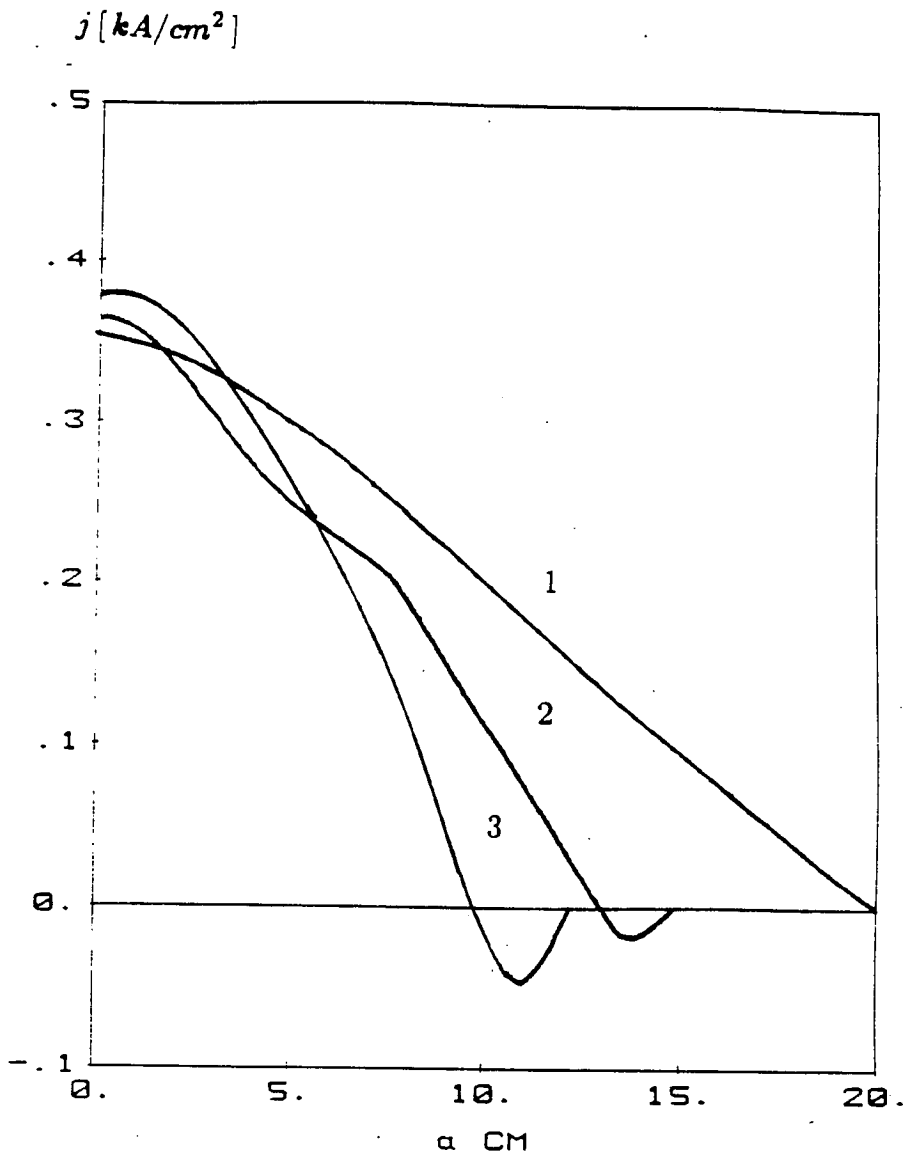


**Fig.**6

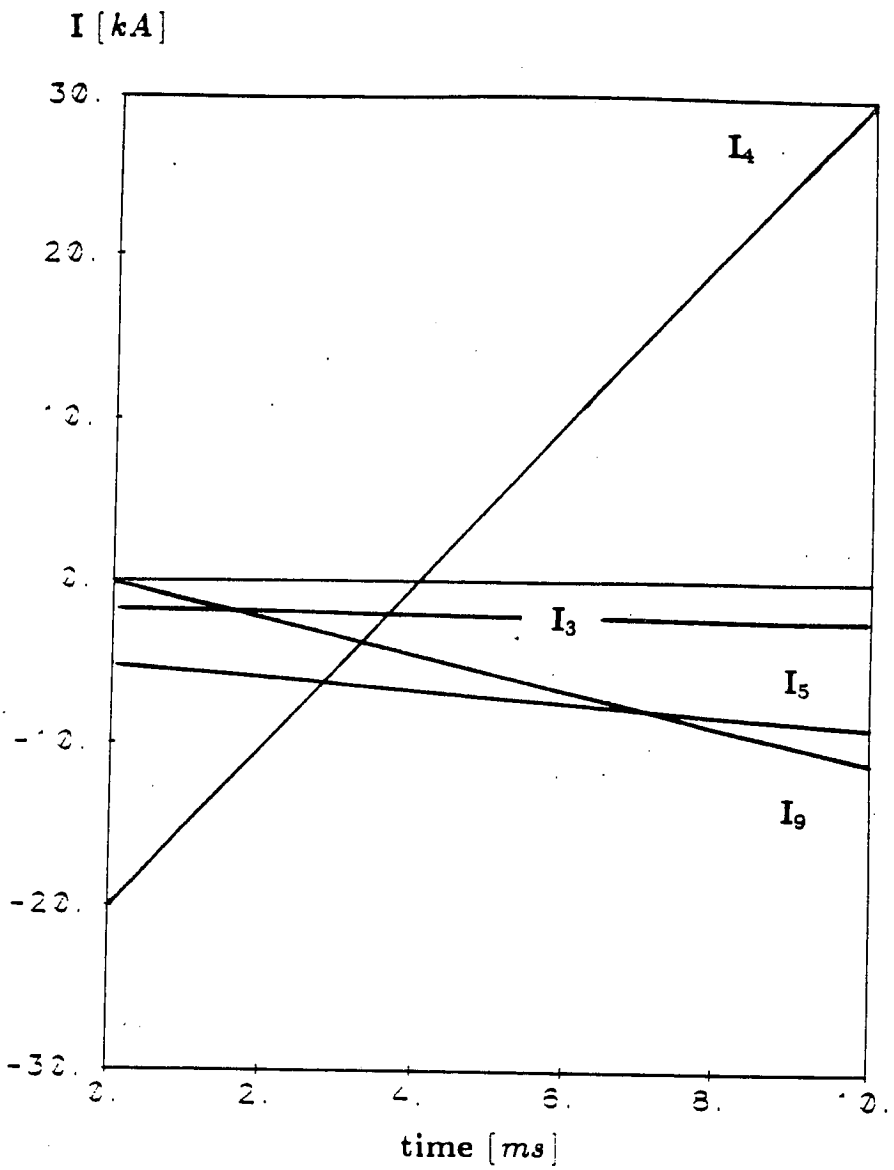


**Fig.7**

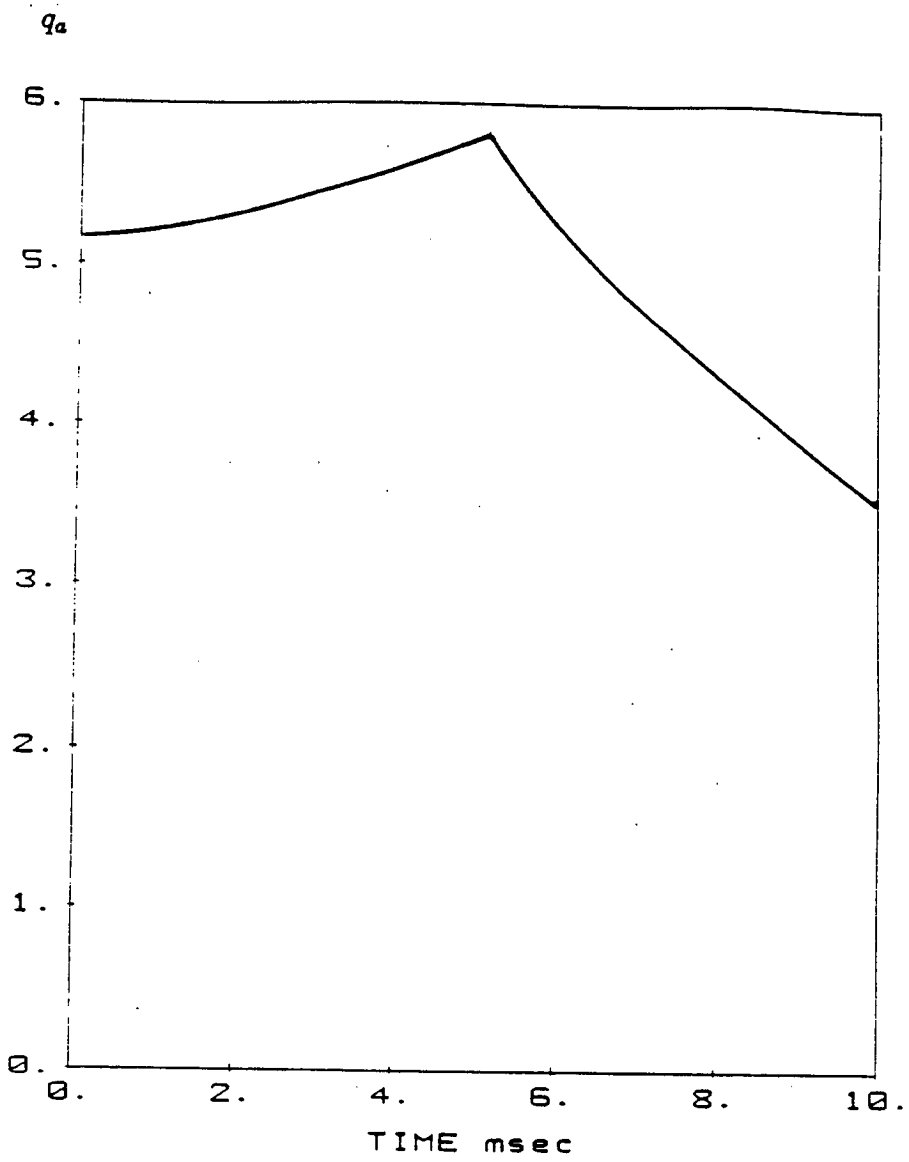


**Fig.**8

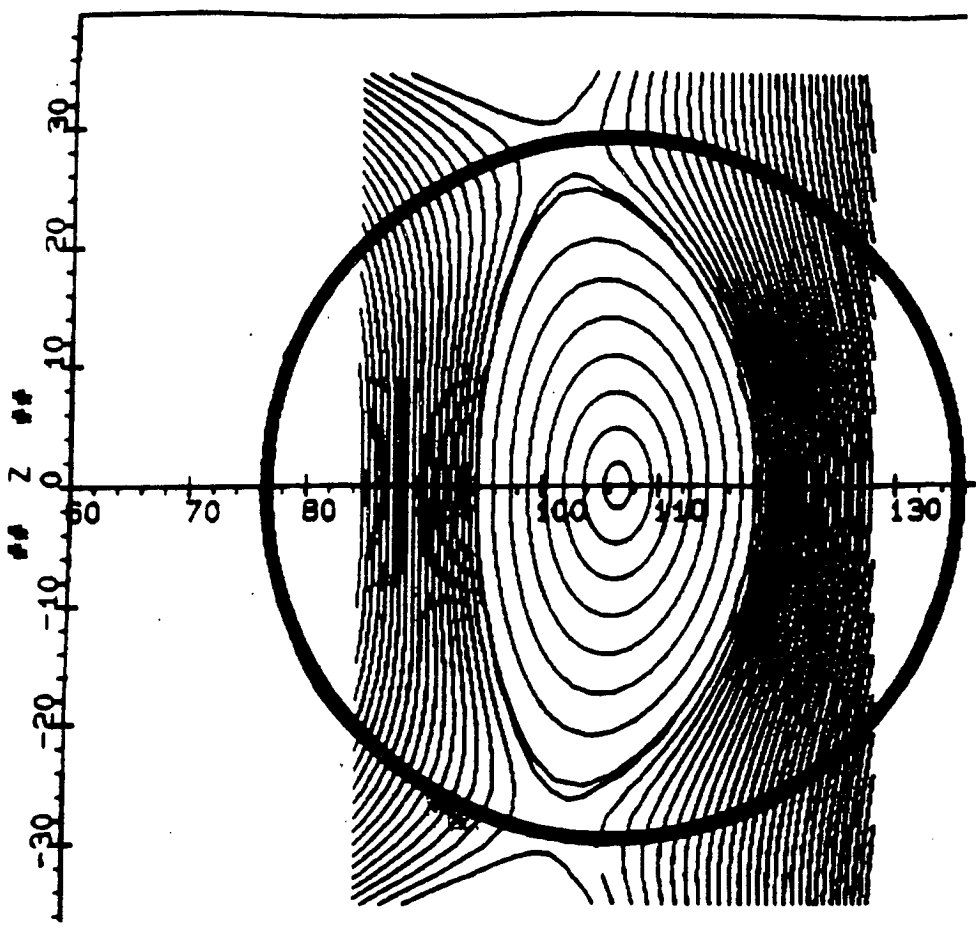


Fig.9